PROCEEDINGS OF SCIENCE

# ATLAS Forward Proton Detectors Status and Plans

**Paula Erland, on behalf of the ATLAS Collaboration**[*†]
*The Henryk Niewodniczański Institute of Nuclear Physics Polish Academy of Sciences, Cracow, Poland*
*E-mail:* paula.erland@ifj.edu.pl

A brief description of the ATLAS Forward Proton detectors is given. The detectors are intended to measure protons scattered at very small angles – a typical signature of diffractive physics. The main features of the AFP detector are presented: the Roman pot technology, Silicon Tracker (SiT) and time-of-flight (ToF) detectors. The performance of the SiT is presented and discussed.

ATL-FWD-PROC-2019-001
06 February 2019

*The 27th International Workshop on Vertex Detectors – VERTEX2018*
*22-26 October 2018*
*MGM Beach Resorts, Muttukadu, Chennai, India*

[*]Speaker.

[†]The work of P.E. has been partially supported by the 'Diamentowy Grant' programme reg. no DI2016 013846 (0138/DIA/2017/46).

## 1. Introduction

Located at the Large Hadron Collider (LHC) [1], the ATLAS experiment [2] has been designed with the goal of measuring the products of proton–proton collisions. Although it has a full azimuthal angle coverage and a large acceptance in pseudorapidity, it is not fully sufficient for a certain group of physics processes, in particular the diffractive ones.

These processes can be characterised by a presence of rapidity gap(s) (a region in rapidity devoid of produced particles) and the scattered proton(s) which preserve their identity. This is due to the nature of such interactions in which the exchanged object is a colour singlet. For electromagnetic interactions such an object is a photon whereas for strong ones it is Pomeron (in QCD: two gluons + h.o. terms).

Diffractive protons are scattered at very small angles (few hundred $\mu$rad), i.e. they escape into the LHC beam pipe. Examples of diffractive (double Pomeron exchange jet production, left) and Beyond Standard Model (anomalous quadric gauge couplings, right) processes are presented in Figure 1.

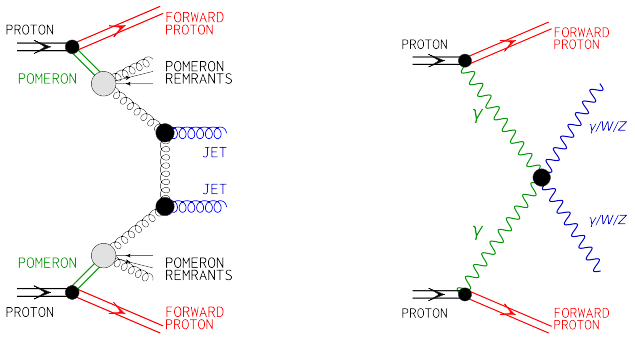


Figure 1: **Left:** double Pomeron exchange di-jet production. **Right:** anomalous quartic gauge couplings.

Characteristic features of diffractive processes allow two methods of their detection. The first one is focusing on studies of the rapidity gap. It is a classical recognition method. Unfortunately, the gap may be destroyed by e.g. particles from pile-up or may be produced outside the acceptance of the ATLAS central detector. The second method is based on detecting scattered protons. The advantage of this approach is that the protons are measured directly, hence it can be used in the non-zero pile-up environment. However, because protons are scattered at very small angles close to the beam, it requires the additional "forward" detectors to be placed far away from the interaction point.

## 2. AFP Detector

The ATLAS experiment has two sets of the forward proton detectors: Absolute Luminosity For ATLAS (ALFA [3]) and ATLAS Forward Proton (AFP [4]). ALFA is dedicated to the measurements of the elastic scattering [5] performed during special LHC runs and is not the subject of the present paper. The AFP consists of two Roman Pot (RP) stations (called Near and Far) on each

side of ATLAS. They are located about 210 m from the ATLAS Interaction Point (P1) and can be inserted horizontally into the LHC beam pipe in the immediate vicinity of the beams.

In the case of non-stable beams the pots are stored in a "safe" position, which is about 40 mm from the beam. When there is a stable beam flag, the detectors can be located 2-3 mm away from the beam centre. The motor position is cross-checked with the Linear Variable Differential Transformer (LVDT) readout and the movement control is very precise: 5 $\mu$m accuracy.

Each RP consists of four Silicon Tracker (SiT) planes. Additionally, Far stations host the Time of Flight (ToF) detectors. Both detector systems are discussed in detail below. The schematic of the AFP components is shown in Figure 2.

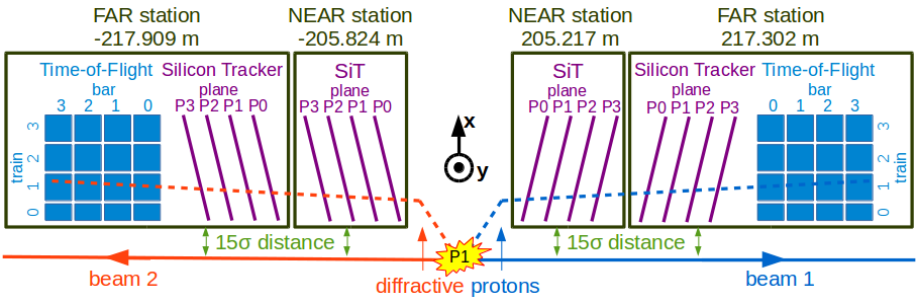


Figure 2: Location of the AFP detectors around the ATLAS interaction point.

## 3. LHC Optics and Proton Trajectories

As it was already mentioned, the diffractive protons are scattered at the very small angles into the LHC beam pipe. They travel through the magnetic lattice of the LHC. In consequence, the proton trajectories between the interaction point and the forward detectors are not straight lines. In fact, there are several LHC elements that influence the proton trajectory. Those are: two dipole magnets (D1, D2) for beam separation (bending), five quadrupole magnets (Q1-Q5) for beam focusing and two collimators (TCL4, TCL5) for the magnet protection.

Settings of these elements is called the accelerator optics and it comes from the requirements of the experiments in terms of luminosity and from the LHC machine protection. Figure 3 shows a typical situation for the high-luminosity ATLAS data taking [6]. The horizontal axis shows the distance along the beam from P1 whereas the vertical one the scattered proton position in $x$ direction: the accelerator (horizontal) plane. The proton trajectories for different relative energy losses, $\xi = 1 - \frac{E_{proton}}{E_{beam}}$, are marked with black lines and the LHC elements are marked as black rectangles for dipole and quadrupole magnets and blue lines for collimators. The red lines show the locations of the AFP and ALFA stations.

The trajectories of protons are bent according to the energy lost during the collision. The scattered protons with $\xi \approx 0$ are very close to the beam and can not be detected by the AFP detectors. With increasing $\xi$ value, the protons move further from the beam and may reach the detectors. For large $\xi$ the proton trajectories will diverge from the beam so far that they hit the beam pipe or the collimators. The acceptance of the AFP detectors for a typical high-luminosity optics spans $0.02 < \xi < 0.1$, which corresponds to the energy loss of a proton of 130 GeV$< E_{proton} <$ 650 GeV for $\sqrt{s} = 13$ TeV.

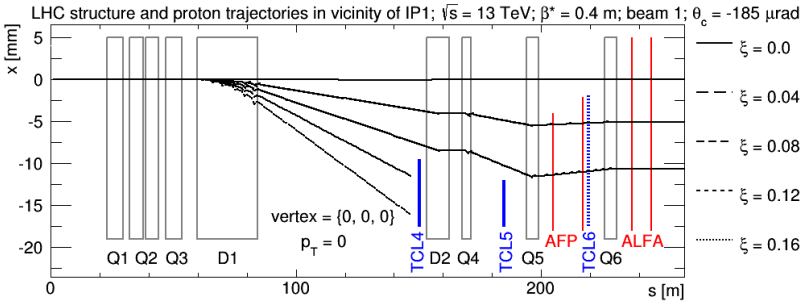


Figure 3: Proton trajectories between the ATLAS interaction point and the AFP detectors, from [6].

### 3.1 Protons in AFP

During the design phase Monte Carlo simulations were used to check the proton visibility in the AFP stations. A simple simulation of the proton transport with a given $\xi$ and the transverse momentum, $p_T$, was performed using the MAD-X [7] programme. Results are presented in Figure 4 (left). The beam is located at (0,0), the circles (squares) represent the positions of protons with $\xi$ = 0 (0.07) and filled and hollow symbols mark different values of $p_T$ accordingly to the azimuthal angle. One can conclude that the protons with higher energy loss are further away from the beam. Presence of non-zero transverse momentum introduces an additional shift in x and y, in the detector plane.

Figure 2-right shows results concerning the detector response and the track reconstruction. Diffractive protons were generated by Pythia 8 [8] and Geant4 transport [9] was used. On this plot a characteristic distribution – the so-called diffractive pattern – is clearly visible.

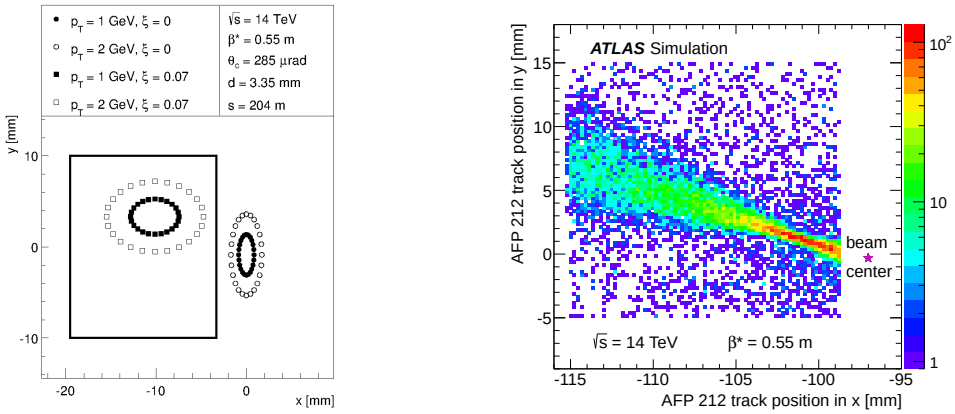


Figure 4: Simulated proton position in the AFP detector. **Left:** protons with given $\xi$ and $p_T$ (from [6]). **Right:** simulation of the detector response and the track reconstruction (from [4]).

### 3.2 AFP Acceptance

In the AFP case one considers the geometric and the produced diffractive mass acceptances. The first is defined as the ratio of the number of protons of a given $(\xi, p_T)$ reaching the AFP to the total number of scattered protons having such $\xi$ and $p_T$ values. An example of the geometric acceptance of one of the AFP stations is presented in Figure 5. The black region means that more than 80% of the scattered protons will hit AFP. The two noticeable $\xi$ limits where discussed before and are due to beam-detector distance (lower limit) and collimator settings (upper limit).

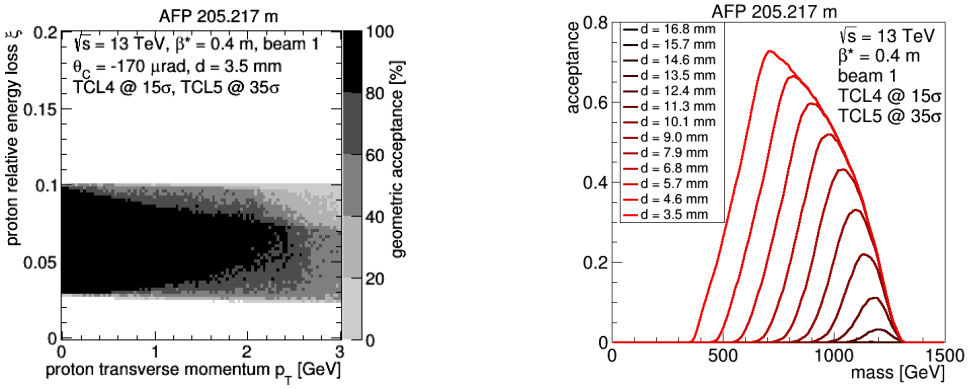


Figure 5: Near station acceptance: geometric (left) and mass (right). From [4].

The mass acceptance is defined as the probability that both protons scattered in a process leading to a production of a central system of a given mass will be visible in AFP. One can observe (see Figure 5, right) that if a hypothetical particle of a mass of 700 GeV is exclusively (i.e. no other particles) produced in the pp collision, there is a 70% chance to observe the scattered protons in the AFP detectors if they are inserted 3.5 mm from the beam.

## 4. AFP Silicon Detectors

The AFP pixelated Silicon Tracking (SiT) system provides the position measurement of the scattered protons. Each station is equipped with four SiT modules tilted by 14°. A single module consist of 336×80 pixels with a pixel size of 50×250 $\mu$m$^2$ with thickness of 230 $\mu$m. The dead edge from the beam side is only ∼100 $\mu$m. Detectors are expected to withstand a non-uniform radiation with fluence of $3 \cdot 10^{15}$ $n_{eq}/$ cm$^2$ per 100 fb$^{-1}$. The read-out is performed by the FE-I4B front-end chip [10] which uses a 40 MHz external clock. The FE-I4B is also capable of triggering the system.

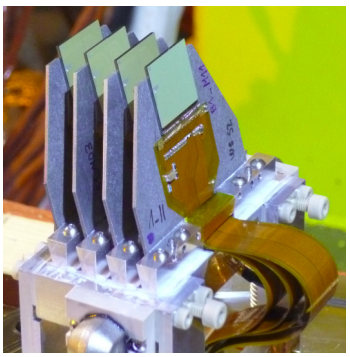

Figure 6: Four AFP Silicon Tracker detectors mounted on the heat exchanger.

Diffractive protons move almost in parallel to the beam. Their trajectory slope is about 20 $\mu$rad [6]. If SiT planes would be perpendicular to the beam then they would have resolution of $50/\sqrt{12}$ $\mu$m. This can be improved by tilting the detector, which

causes charge sharing between the pixels, thereby improving the resolution. For AFP the optimum was found at 14° – the spacial resolution of a single plane was measured to be 6 $\mu$m [11].

### 4.1 First Data-Taking

AFP successfully took data since 2016. In the first year, the detectors were only inserted during special, low luminosity runs. Since 2017 the AFP has taken data in all regular LHC fills. In 2017 AFP collected 32.0 fb$^{-1}$ of data and in 2018 49.3 fb$^{-1}$. Some basic performance plots are shown in Figure 7: the hit pattern (left), the pixel hit multiplicity (centre) and the correlation between neighbouring pixel planes (right). As expected from the simulation, a diffractive pattern is clearly visible. The activity in region of 4<y<10 mm and x∼0 is due to the beam halo. It is worth stressing that these data were taken during the Beam Based Aligment procedure when the detectors were almost touching the beam. The pixel multiplicity peaks at 2. The small excess at 4 is due to double proton hits. A good correlation between adjacent SiT planes indicates the dominance of diffractive proton tracks.

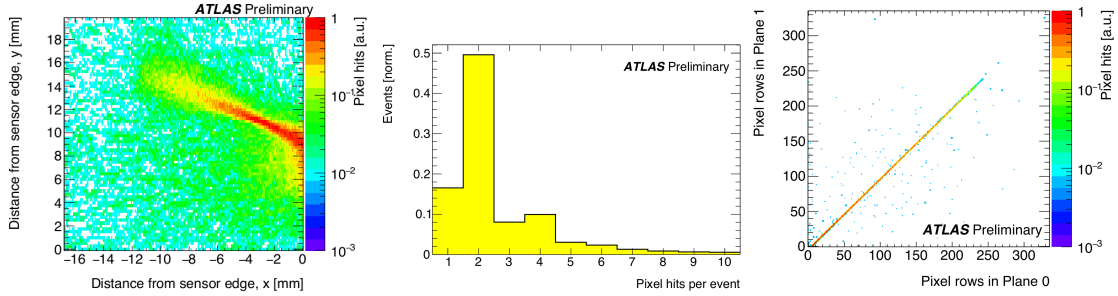


Figure 7: **Left:** diffractive pattern + beam halo visible in the AFP Far station during the Beam-Based-Alignment procedure. **Middle:** pixel multiplicity during the data taking. **Right:** correlation of raw unclustered pixel hits between two consecutive tracker planes in events with maximally 2 hits per plane (from [12]).

### 4.2 Running Conditions and Radiation Damage

Operation in the high-luminosity environment causes radiation damage to the silicon sensors and the readout chips. The damage is proportional to the integrated luminosity and is visible e.g. in the increase of the Low Voltage (chip) current see Figure 8. In the absence of the beams, the local radiation dies out: the SiT modules recover, which results in a drop of the LV current.

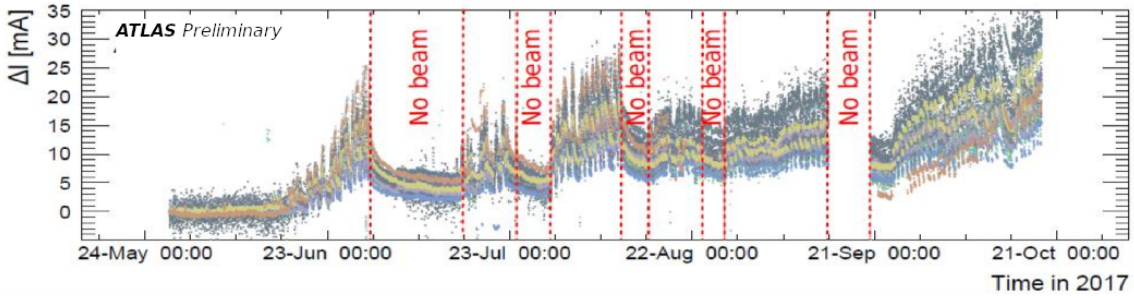


Figure 8: Low Voltage current of SiT modules in 2017.

The performance of irradiated modules strongly depends on the temperature of the chip and is related to the High Voltage leakage current. This relation is shown in Figure 9. The chosen working temperature for the AFP SiT modules is around -20°C. Such a low temperature is achieved by the AFP cooling system based on Vortex Tube technology [4], which provides cooling down to -25°C with detectors powered on. For regulation a Proportional-Integral-Derivative (PID) algorithm is used. For machine safety (in case the thin pot window would brake) and to decrease risk of icing a secondary vacuum system was installed.

The secondary vacuum is kept between 5 and 30 mbar. Its presence solves also another problem which is the mechanical stress (due to atmospheric pressure) on the thin window and floor of the Roman pot [4].

At the end of the 2017 data taking period, after collecting 32 fb$^{-1}$ data, studies of the AFP efficiency were performed. In Figure 10 (left) the efficiency for the three different occupancy regions with different track multiplicities as a function of the bias voltage are shown. The occupancy regions are: high – above 70%, medium – between 30 and 70% and low – below 30%. As one can see, full efficiency is reached for a bias voltage larger than 30 V.

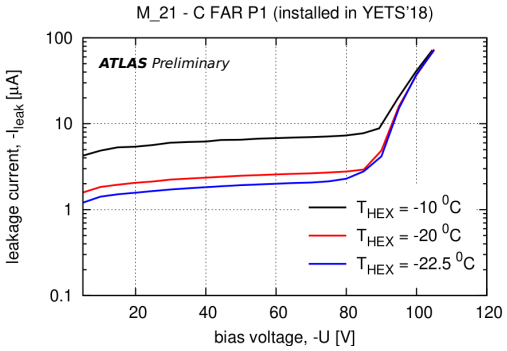


Figure 9: Leakage current in station C Far module P1 as a function of bias voltage for different temperatures.

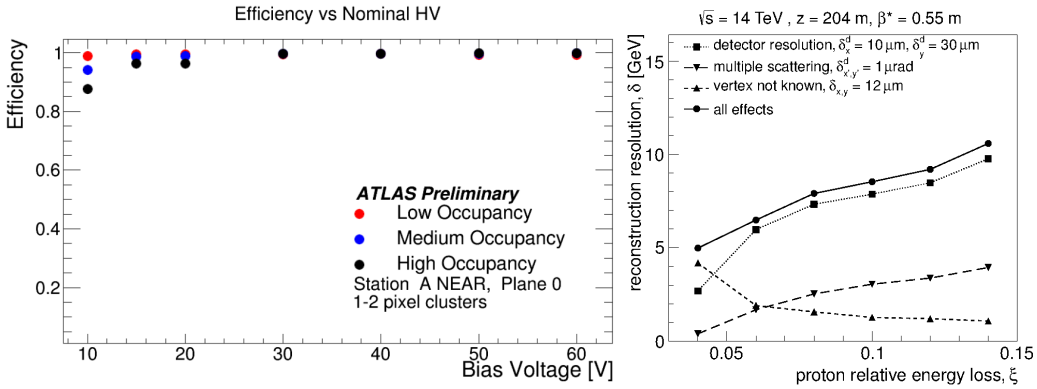


Figure 10: **Left:** AFP efficiency in function of bias voltage for three different occupancies (from [13]). **Right:** reconstruction resolution in function of $\xi$ for different effects (from [4]).

### 4.3 Kinetic Reconstruction Efficiency

The kinematics of the scattered protons is strictly related to that of the central system. Hence it is possible to get the information about the proton kinematics at the IP from optics and position of the hit in the AFP detector. In Figure 10 (right) the reconstruction resolution of the proton relative energy loss received from simulations is presented. The detector spatial resolution plays a major

role. It is visible that when all the effects (continuous line) are considered the expected resolution ranges between 5 and 10 GeV.

## 5. AFP Time-of-Flight Detector

The main backgrounds for the discussed physics of interest are non-diffractive and single diffractive process as with protons originating from pile-up. These backgrounds can be significantly reduced by using the Time of Flight detectors.

The idea is to measure the difference of the time of flight of the scattered protons on both sides of the ATLAS IP: $(t_A - t_C)$, and to compare it to the location of the vertex reconstructed by ATLAS: $(t_A - t_C) \cdot c/2 - z_{ATLAS}$. Since several pp interactions in a single bunch-crossing are expected during the regular ATLAS data-taking, the probability of combinatorial background is high. The AFP Time-of-Flight detector was designed to reduce such a background by a factor of $\sim$10, see Figure 11. The black line represents the expected background reduction due to the AFP proton tag and blue and red lines represent the background with timing measurement included.

AFP ToF detector is composed of 16 L-shaped quartz bars (see Figure 12, left). When a scattered proton hits these bars, the created Cherenkov light is guided to a Micro-Channel Plate Photo-Multiplier (MCP-PMT). After the amplification, the readout is carried out by the radiation hard electronics.

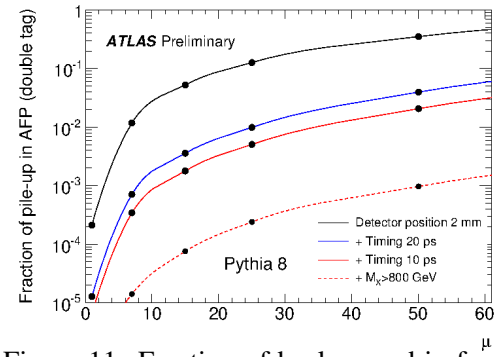


Figure 11: Fraction of background in function of pile-up (from [4]).

Studies of the ToF time resolution were performed during the beam tests. The results from 2015 [11] are shown in Figure 12 right. The time resolutions were measured as the time differences between one bar and one of the SiPM references. The time resolutions of the full ToF including the readout contributions were measured to be (at 1900 V) between: 38 $\pm$ 6 ps and 46 $\pm$ 5 ps per LQbar and 35 $\pm$ 6 ps and 37 $\pm$ 6 ps per train.

## 6. Summary

The ATLAS Forward Proton detectors are placed in both outgoing LHC beams at 210 m from the ATLAS interaction point. The AFP detectors are inserted horizontally into the beam pipe exploiting the Roman Pot technology. Each RP contains four Silicon Tracker planes. The structure of the SiT detectors was discussed including the motivation for the tilt of the silicon modules. The radiation damage during 2017 and leakage current were presented.

Stations located farthest from ATLAS interaction point also host Time of Flight detectors. The main goal of ToF modules is to reduce pile-up, the rate of witch grows with increasing number of pp interactions per bunch crossing. Studies of ToF time resolution were shown. The beam test results show that the resolution is expected to be 20 - 50 ps.

The AFP detector, taking part at std. lum running, should provide possibilities of new studies of central exclusive production and anomalous quartic gauge boson couplings.

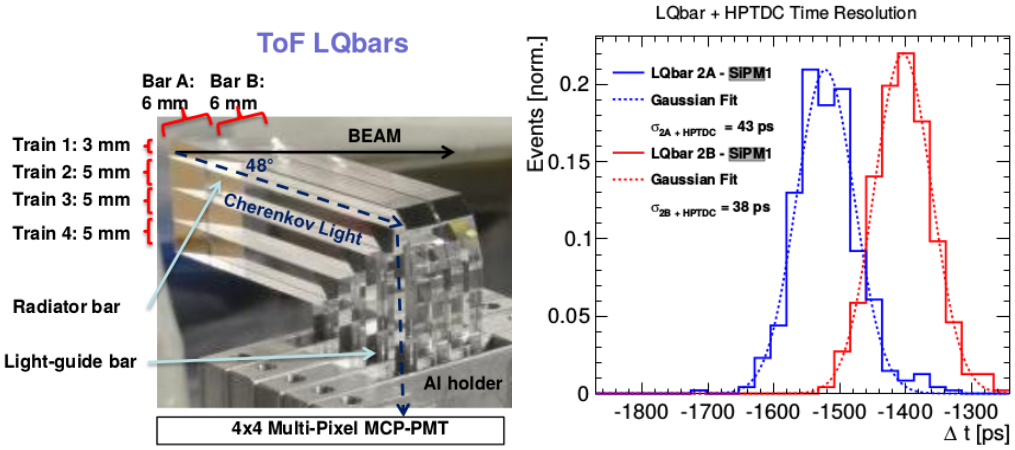


Figure 12: Left: ToF modules. Right: the time differences between the LQbars of the second train (2A and 2B) and SiPM1 (from [11]).

## References


[1] L. Evans and P. Bryant, *LHC Machine*, JINST 3 (2008) S08001.

[2] ATLAS Collaboration, *The ATLAS Experiment at the CERN Large Hadron Collider*, JINST 3 (2008) S08003.

[3] ATLAS Collaboration, *ATLAS Forward Detectors for Measurement of Elastic Scattering and Luminosity*, ATLAS TDR 018, CERN/LHCC 2008-04.

[4] ATLAS Collaboration, *Technical Design Report for the ATLAS Forward Proton Detector*, CERN-LHCC-2015-009, ATLAS-TDR-024.

[5] ATLAS Collaboration, *Measurement of the total cross section from elastic scattering in pp collisions at* $\sqrt{s} = 8$ *TeV with the ATLAS detector*, Phys. Lett. B 761 (2016) 158.
ATLAS Collaboration, *Measurement of the total cross section from elastic scattering in pp collisions at* $\sqrt{s} = 7$ *TeV with the ATLAS detector* , Nuclear Physics B (2014) 486.

[6] M. Trzebiński, *Machine Optics Studies for the LHC Measurements*, Proc. SPIE 9290 (2014) 929026.

[7] F. Schmidt, *MAD-X User's Guide*, CERN 2005.

[8] R. Ciesielski and K. Goulianos, *MBR Monte Carlo Simulation in PYTHIA8*, arXiv:1205.1446.

[9] S. Agostinelliae, J. Allisonas, K. Amako et al., *Geant4 – a simulation toolkit*, A 506 (2003) 250-303.

[10] ATLAS IBL Collaboration, *Prototype ATLAS IBL Modules using the FE-I4A Front-End Readout Chip*, JINST 7 (2012) P11010.

[11] J. Lange et. al. *Beam tests of an integrated prototype of the ATLAS Forward Proton detector*, JINST 11 (2016) P09005.

[12] https://twiki.cern.ch/twiki/bin/view/AtlasPublic/ForwardDetPublicResults#AFP_figures .

[13] C. Grieco, *ATLAS Forward Proton Detector*, ATL-FWD-PROC-2018-005, https://cds.cern.ch/record/2640536/?ln=pl .